
GAC: Stabilizing Asynchronous RL Training for LLMs via Gradient Alignment Control

Haofeng Xu^{1,2} Junwei Su^{1†} Yukun Tian^{3,2} Lansong Diao² Zhengping Qian² Chuan Wu^{1†}

Abstract

Asynchronous execution is essential for scaling reinforcement learning (RL) to modern large-model workloads, including large language models and AI agents, but it can fundamentally alter RL optimization behavior. While prior work on asynchronous RL focuses on training throughput and distributional correction, we show that naively applying asynchrony to policy-gradient updates can induce qualitatively different training dynamics and lead to severe training instability. Through systematic empirical and theoretical analysis, we identify a key signature of this instability: asynchronous training exhibits persistently high cosine similarity between consecutive policy gradients, in contrast to the near-orthogonal updates observed under synchronized training. This *stale-aligned gradient* effect amplifies correlated updates and increases the risk of overshooting and divergence. Motivated by this observation, we propose GRADIENT ALIGNMENT CONTROL (GAC), a simple dynamics-aware stabilization method that regulates asynchronous RL progress along stale-aligned directions via gradient projection. We establish convergence guarantees under bounded staleness and demonstrate empirically that GAC recovers stable, on-policy training dynamics and matches synchronized baselines even at high staleness.

1. Introduction

Reinforcement learning (RL) provides a principled framework for optimizing large language models (LLMs) as decision-makers, where text generation is modeled as a sequence of actions and learning is driven by feedback on com-

plete responses rather than token-level supervision (Zhang et al., 2025; Wang et al., 2025a). Unlike supervised pre-training, RL enables LLMs to learn from delayed, outcome-based signals—such as human preferences, task success, or correctness—allowing models to improve behaviors that are difficult or impossible to specify with static annotations. In modern alignment pipelines, policy-gradient methods such as Group Relative Policy Optimization (GRPO) (Shao et al., 2024) train an LLM by sampling multiple candidate responses to the same prompt and reinforcing those that achieve higher relative reward within the group, thereby directly optimizing response-level quality and reasoning performance. This RL-based fine-tuning paradigm has become central to aligning LLMs with human intent, improving mathematical and logical reasoning, and adapting pre-trained models to complex, open-ended tasks where explicit supervision is unavailable or insufficient (Feng et al., 2025).

Despite this algorithmic flexibility, the scalability of RL for LLMs is increasingly constrained by *system-level bottlenecks* rather than by limitations of the learning algorithms themselves (Sheng et al., 2024; Zhong et al., 2025). A typical RL training pipeline consists of several heterogeneous stages—rollout generation via model inference, reward and advantage computation, and policy optimization—that operate on different time scales and often rely on distinct hardware resources. In LLM settings, rollout generation is frequently dominated by inference latency and sampling throughput, whereas policy optimization is compute-intensive and highly optimized on accelerators. As model sizes and deployment scales grow, enforcing strict synchronization across these stages leads to significant underutilization of resources (Fu et al., 2025; Wang et al., 2025b). Fully synchronous policy-gradient methods such as GRPO execute these stages in lockstep, requiring all workers to complete rollout collection and preprocessing (e.g., reward computation) before any policy update can proceed. In large-scale distributed systems, this design exacerbates straggler effects caused by variable rollout lengths, heterogeneous hardware, and resource contention, resulting in substantial idle time and poor wall-clock efficiency (Sheng et al., 2025).

To alleviate these issues, modern RL systems increasingly

[†]Corresponding authors. ¹Department of Computer Science, The University of Hong Kong, Hong Kong SAR, China ²Alibaba Group, China ³Southeast University, Nanjing, China. Correspondence to: Junwei Su <junweisu.cs@gmail.com>, Chuan Wu <cwu@cs.hku.hk>.

adopt asynchronous training, in which rollout generation and policy optimization proceed concurrently. While this relaxation of synchronization is essential for scaling RL to large models and high-throughput deployments, it also fundamentally alters the learning dynamics of policy optimization—introducing new sources of bias and instability that must be carefully understood and controlled.

Limitations and Gaps in Existing Work. There has been growing interest in asynchronous RL as a means of addressing the scalability challenges of modern large-scale systems. However, existing efforts leave a critical gap in understanding and controlling the *learning dynamics* induced by asynchrony. Broadly, prior work falls into two categories. The first line of research is *systems-oriented* (Fu et al., 2025; Sheng et al., 2025; Lu et al., 2025): it focuses on exploiting the engineering benefits of asynchrony—such as mitigating stragglers, improving hardware utilization, and maximizing throughput under asynchronous execution. These approaches typically treat the learning algorithm as a black box and devote limited attention to how stale rollouts and delayed updates fundamentally alter the underlying training process. The second line is *algorithm-oriented* (Xi et al., 2025; Zheng et al., 2025; Li et al., 2026): it develops asynchronous RL methods from a largely system-agnostic perspective. They primarily emphasize *distributional corrections* to reduce the mismatch between the on-policy distribution in synchronous training and the off- or stale-policy distributions induced by asynchrony. While such corrections can be effective when training dynamics remain stable and free from collapse, they overlook a more fundamental issue: asynchronous and synchronous training can exhibit *qualitatively different training dynamics*. As we demonstrate in this paper, naïvely applying asynchronous execution to GRPO-style updates—without explicitly accounting for the resulting training dynamics—can lead to severe instability and even training collapse.

Contributions. Motivated by these observations, we study asynchronous RL from an underexplored *training-dynamics perspective*. We characterize the key dynamical differences between synchronous and asynchronous policy training that give rise to training instability and collapse, and we identify a simple yet effective control mechanism that directly targets these dynamics. Our approach intervenes at the level of training behavior rather than solely correcting distributional shift, providing both theoretical insight and practical stability improvements. Our main contributions are summarized as follows:

1. **Characterization of asynchronous training dynamics.** We conduct a systematic empirical comparison between synchronous and asynchronous reinforcement learning and uncover two consistent findings. First, un-

der comparable hyperparameters, asynchronous training is substantially more prone to *collapse* than its synchronous counterpart. Second, this instability is associated with a sharp dynamical distinction

captured by the *cosine similarity* between consecutive policy gradients. Contrary to the behavior commonly observed in supervised learning, synchronous RL often exhibits *low* cosine similarity across successive gradients, indicating diverse descent directions over time, whereas asynchronous RL exhibits persistently *high* cosine similarity. This alignment provides an explanation for instability: gradient staleness in asynchronous execution repeatedly reinforces similar update directions, increasing the risk of overshooting and divergence. We further support this empirical observation with a theoretical analysis (Theorem 3.1) showing that stale gradients introduce a systematic bias that increases gradient alignment and fundamentally alters the convergence behavior of asynchronous RL.

2. **A dynamics-aware stabilization method with convergence guarantees.** Motivated by the above findings, we propose GAC (Gradient Alignment Control), a simple yet effective mechanism for stabilizing asynchronous reinforcement learning by explicitly regulating its progress along stale-aligned update directions. GAC leverages the cosine similarity between consecutive policy gradients to adaptively project the current gradient relative to the previous update and modulate the effective gradient direction, thereby preventing excessive movement along highly correlated directions that can lead to overshooting and instability. We provide theoretical analysis (Proposition 4.1) showing that GAC can reduce alignment-induced bias and improve the convergence stability of asynchronous RL. Importantly, GAC is algorithm- and system-agnostic, and can be readily integrated with existing RL algorithms and distributed training systems to stabilize large-scale asynchronous RL training.
3. **End-to-end improvements in asynchronous GRPO training.** We evaluate GAC in large-scale asynchronous GRPO training across Qwen3 models ranging from 1.7B to 8B parameters and seven mathematical reasoning benchmarks. Under moderate to large staleness, naïve asynchronous GRPO (and baselines) exhibits unstable dynamics and frequent performance collapses. In contrast, GAC consistently stabilizes training, restores on-policy-like optimization behavior, and substantially closes the performance gap to synchronized GRPO, while preserving the throughput benefits of asynchronous execution. These results demonstrate that explicitly controlling gradient alignment is both necessary and sufficient for stabilizing large-scale asynchronous GRPO in practice.

2. Preliminaries

2.1. Group-Relative Policy Optimization (GRPO)

GRPO is a policy-gradient method designed for reinforcement learning with outcome-level or verifier-based rewards, and is widely used in large language model post-training. GRPO follows the clipped-surrogate optimization framework of Proximal Policy Optimization (PPO) (Schulman et al., 2017), but replaces value-function-based advantages with a group-relative normalization computed over multiple responses to the same prompt.

Let $\pi_\theta(a | s)$ denote a stochastic policy parameterized by θ , and π_{θ_b} denote the behavior policy used to generate training data. For a sampled state–action pair (s, a) , define the importance ratio

$$r_\theta(s, a) \triangleq \frac{\pi_\theta(a | s)}{\pi_{\theta_b}(a | s)}.$$

Given an advantage estimate A , GRPO adopts the PPO clipped surrogate

$$\ell_\varepsilon(r, A) \triangleq \min(rA, \text{clip}(r, 1 - \varepsilon, 1 + \varepsilon)A).$$

For a prompt or context $c \sim \mathcal{D}$, GRPO samples a group of G trajectories $\{\tau^{(g)}\}_{g=1}^G$, producing scalar returns $\{R^{(g)}\}_{g=1}^G$. The group-relative advantage is defined as

$$A_b^{(g)} \triangleq \frac{R^{(g)} - \mu_G}{\sigma_G + \varepsilon},$$

where μ_G and σ_G are the mean and standard deviation of the returns within the group. This normalization serves as an implicit control variate, reducing gradient variance without requiring a learned value function.

Let $d_{\pi_{\theta_b}}(s, a | c)$ denote the discounted state–action visitation distribution induced by the behavior policy under context c . The GRPO objective is given by

$$\mathcal{L}_{\text{GRPO}}(\theta) = \mathbb{E}_{c \sim \mathcal{D}} \left[\frac{1}{G} \sum_{g=1}^G \mathbb{E}_{(s,a) \sim d_{\pi_{\theta_b}}(\cdot | c)} [\ell_\varepsilon(r_\theta(s, a), A_b^{(g)})] \right].$$

The clipping operation enforces a trust-region–like constraint on policy updates, while group-relative normalization provides context-aware credit assignment suitable for sparse or outcome-based rewards.

2.2. Synchronous and Asynchronous GRPO Training

We distinguish between *synchronous* and *asynchronous* execution of GRPO by whether rollout generation and policy optimization are coupled, consistent with standard distributed RL pipelines (Mnih et al., 2016; Espeholt et al., 2018).

In *synchronous GRPO*, rollout generation and optimization proceed in lockstep. At update step t , trajectories are generated using the current policy π_{θ_t} , and the aggregated policy gradient

$$g_t \triangleq \nabla_\theta \mathcal{L}_{\text{GRPO}}(\theta_t)$$

is computed from on-policy data. The policy parameters are updated as

$$\theta_{t+1} = \theta_t + \eta g_t,$$

where $\eta > 0$ is the learning rate. In this regime, gradients are evaluated under the current policy distribution, and standard on-policy optimization behavior is observed.

In *asynchronous GRPO*, rollout generation is decoupled from optimization to improve system throughput. At optimization step t , the data batch may be generated by a stale behavior policy $\pi_{\theta_{t-\tau}}$, where $\tau \geq 0$ denotes the staleness induced by pipeline delays and straggler effects. The learner update takes the form

$$\theta_{t+1} = \theta_t + \eta \hat{g}_t,$$

where \hat{g}_t is a stochastic gradient estimator constructed from trajectories sampled under $d_{\pi_{\theta_{t-\tau}}}$.

Asynchronous execution decouples rollout generation from policy optimization to maximize throughput, but fundamentally transforms GRPO into an off-policy procedure. Although the behavior policy is corrected by importance ratios in the GRPO objective at the surrogate level, asynchrony introduces a fundamental discrepancy: gradients are evaluated under a lagged distribution rather than the current policy. Prior work attributes such off-policy failures primarily to distributional mismatch, which erodes the local validity of surrogate objectives and manifests as trust-region violations (e.g., KL divergence spikes, elevated clip fractions). This staleness further induces systematic bias and temporal coupling between successive updates, which does not arise in synchronized training and can qualitatively alter optimization dynamics. Understanding and controlling the resulting training behavior is the central focus of this work.

3. Training Dynamics of Asynchronous RL

In this section, we present one of the central findings of this paper: asynchronous and synchronous RL exhibit *qualitatively different training dynamics*. We begin with an empirical study demonstrating that staleness introduced by asynchronous execution can induce catastrophic instability in policy optimization. We then show that this instability is consistently preceded by a clear dynamical signature—persistent alignment between consecutive policy gradients—captured by their cosine similarity. In contrast, synchronized RL typically exhibits low inter-gradient similarity, with near-orthogonal update directions. Finally, we provide a theoretical analysis that grounds these empirical observations, showing how gradient staleness induces alignment and fundamentally alters the convergence behavior of asynchronous RL.

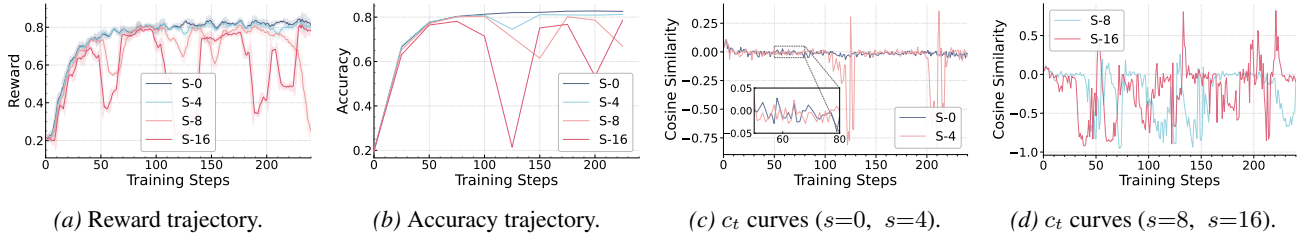


Figure 1. **Progressive instability under increasing staleness.** Panels (a–b) report training reward and validation accuracy across staleness levels. Panels (c–d) report consecutive-gradient cosine similarity c_t , contrasting synchronized training ($s=0$) with mild ($s=4$) and larger staleness ($s=8, 16$). Results on MATH with Qwen3-4B.

3.1. Staleness Induces Catastrophic Instability

We study the effect of staleness by varying $s \in \{0, 4, 8, 16\}$, where s denotes the number of optimization steps by which the behavior policy lags behind the learner policy. We define *training collapse* as a failure mode in which learning dynamics become persistently unstable, leading to sustained degradation or oscillatory behavior that precludes reliable convergence. In practice, collapse is characterized by the following: (i) sharp drops in validation accuracy with no subsequent recovery over extended training, and (ii) reward trajectories that stagnate or exhibit large-amplitude, recurrent fluctuations. Figure 1 (a)–(b) show the resulting degradation in training behavior as staleness increases. Synchronized training ($s=0$) exhibits stable, well-behaved convergence. Even a small amount of staleness ($s=4$) introduces mild non-stationarity, with noticeable but limited fluctuations in both reward and accuracy. At $s=8$, these fluctuations grow into large-amplitude oscillations that repeatedly disrupt learning progress. At $s=16$, training becomes markedly unstable: reward and accuracy undergo severe drops and sustained oscillations, preventing reliable convergence. This progressive degradation reveals a fundamental stability limitation of asynchronous GRPO under staleness, motivating the need for explicit stabilization.

3.2. Gradient Alignment as a Dynamical Signature

Having established that asynchronous GRPO can fail catastrophically, we now identify *what distinguishes stable and unstable training dynamics*. To this end, we introduce the *consecutive-gradient cosine similarity*

$$c_t \triangleq \frac{\langle \hat{g}_t, \hat{g}_{t-1} \rangle}{\|\hat{g}_t\|_2 \|\hat{g}_{t-1}\|_2}, \quad (1)$$

where \hat{g}_t denotes the aggregated policy gradient estimate used at update step t , computed from the update batch and potentially induced by staled rollout policy (see Appendix A.1). This metric captures whether successive updates explore diverse descent directions ($|c_t| \approx 0$) or repeatedly reinforce similar directions ($|c_t| \approx 1$).

Distinct cosine-similarity behavior under synchronous and asynchronous training. We empirically find that

consecutive-gradient cosine similarity exhibits a clear qualitative difference between synchronous and asynchronous RL, as illustrated in Figure 1 (c)–(d). In synchronous RL, cosine similarity remains tightly concentrated near zero throughout training, indicating that consecutive policy-gradient updates are nearly orthogonal and explore diverse descent directions—behavior that is stable across training stages and model scales (additional on-policy results across model sizes are provided in Appendix D). In contrast, asynchronous RL exhibits persistently large-magnitude cosine similarity: under staleness, $|c_t|$ departs from zero and becomes markedly more volatile. Even at mild staleness ($s=4$), $|c_t|$ occasionally exhibits abrupt spikes, which are followed by noticeable drops in reward and accuracy. At larger staleness ($s=8$ and $s=16$), cosine similarity oscillates with very large amplitude over extended periods, indicating repeated reinforcement of similar update directions. This sustained alignment provides a mechanistic explanation for training collapse: correlated updates amplify effective step sizes along a low-dimensional subspace, causing errors to accumulate, overshoot the trust region, and trigger divergence. Crucially, the rise in $|c_t|$ consistently *precedes* reward collapse, identifying gradient alignment as a leading indicator—and likely a causal driver—of instability rather than a consequence of failure. Together, these observations establish consecutive-gradient alignment as a robust stability signature distinguishing synchronous from asynchronous training dynamics and motivating explicit alignment control in asynchronous RL.

3.3. Theoretical Evidence

We now show that the empirical gradient-alignment phenomenon admits a direct theoretical explanation. The key observation is that asynchronous execution fundamentally changes the structure of the stochastic gradient update. In particular, stale rollouts can introduce a *persistent bias* that couples consecutive gradients, causing the optimization trajectory to deviate from standard descent behavior.

Theorem 3.1 (Convergence of Asynchronous GRPO, Informal). *Under standard smoothness and bounded-variance assumptions, and assuming locally bounded parameter drift*

induced by staleness, the iterates satisfy

$$\begin{aligned} \min_{0 \leq t \leq T-1} \mathbb{E} \|\nabla \mathcal{L}(\theta_t)\|^2 &\leq \frac{2(L^* - \mathcal{L}(\theta_0))}{\eta T} + 2L\eta\sigma^2 + \text{Err}(T) \\ &+ \frac{4L\eta}{T} \sum_{t=0}^{T-1} \mathbb{E} \|b_t\|^2 - \frac{2}{T} \sum_{t=0}^{T-1} \eta \rho_t \lambda_t \mathbb{E} \|\hat{g}_{t-1}\|^2, \end{aligned}$$

where $L^* \triangleq \sup_{\theta} \mathcal{L}(\theta)$, L is the smoothness constant of $\mathcal{L}(\theta)$, σ^2 bounds the variance of the gradient, b_t denotes the staleness-induced bias arising from stale rollouts, and \hat{g}_{t-1} is the stochastic gradient from the previous update. The coefficients ρ_t and λ_t quantify the persistence and strength of temporal coupling induced by staleness, respectively. Under the small-drift linearization, the bias admits the approximation $b_t \approx \eta_{t-1} B_t \hat{g}_{t-1}$, where B_t is a local linear operator mapping parameter staleness into gradient bias. The term $\text{Err}(T)$ collects higher-order remainder terms due to rollout noise and approximation error.

The formal version of Theorem 3.1 and its proof can be found in Appendix E. Theorem 3.1 extends the nonconvex convergence guarantee with two staleness-dependent effects. The term $\sum_t \mathbb{E} \|b_t\|^2$ captures the *magnitude* of the staleness-induced bias and is always detrimental. The final term reflects *temporal coupling*: when the bias aligns with previous gradients, consecutive updates become correlated.

Alignment-induced instability and collapse. Under asynchrony, empirical results show that this temporal coupling strengthens over time, leading to persistent alignment between consecutive gradients. Through the approximation $b_t \approx \eta_{t-1} B_t \hat{g}_{t-1}$, such alignment directly inflates the bias magnitude $\|b_t\|$ as past gradients are repeatedly reinforced. As a result, the bias penalty term $\sum_t \mathbb{E} \|b_t\|^2$ grows and eventually dominates the right-hand side of the bound, overwhelming the descent signal. When this occurs, updates no longer behave as local descent steps, leading to unstable dynamics and training collapse. This transition manifests empirically as a sharp rise in consecutive-gradient cosine similarity immediately preceding performance degradation. The analysis identifies *alignment persistence*—rather than distributional mismatch alone—as the primary driver of instability in asynchronous GRPO. This perspective motivates explicit control of inter-step gradient alignment to suppress bias amplification and prevent collapse, which directly informs the design of our method below.

4. Gradient Alignment Control (GAC)

We propose GAC, a dynamics-aware stabilization mechanism for asynchronous GRPO that explicitly regulates *inter-step gradient alignment* induced by stale rollouts. Unlike prior approaches that operate at the surrogate or distributional level, GAC intervenes directly at the level of the

policy-gradient update. The method monitors the alignment between consecutive gradients and selectively suppresses progress along stale-aligned directions while preserving informative orthogonal components. This intervention breaks the positive feedback loop created by temporal coupling under staleness and restores update geometry closer to that observed in synchronized training. The complete procedure of GAC is presented at Algorithm 1.

4.1. Directional Gradient Projection

The core operation of GAC is a directional projection that rescales gradient components relative to a reference direction. Let v be a nonzero reference vector and $u \triangleq v/\|v\|_2$ its unit direction. Given any gradient g , we decompose it into components parallel and orthogonal to u :

$$g_{\parallel} \triangleq \langle g, u \rangle u, \quad g_{\perp} \triangleq g - g_{\parallel}. \quad (2)$$

GAC applies anisotropic rescaling with directional gains $(\alpha, \beta) \in \mathbb{R}_+^2$:

$$g' \triangleq \alpha g_{\parallel} + \beta g_{\perp}. \quad (3)$$

Choosing $\alpha < \beta$ attenuates progress along the reference direction u while preserving the residual update signal in the orthogonal subspace. This operation can be equivalently written as a rank-one linear transform $g' = (\beta I + (\alpha - \beta)uu^T)g$, highlighting that GAC modifies update geometry rather than gradient magnitude uniformly.

4.2. Adaptive Alignment Control under Stale Rollouts

In asynchronous GRPO, gradients \hat{g}_t are computed from rollouts generated by a stale behavior policy $\pi_{\theta_{t-\tau}}$, which induces temporal coupling across updates. To regulate this effect, GAC tracks the cosine similarity c_t (Eq. 1) between consecutive gradients, which serves as a direct measure of alignment. As shown in Section 3, synchronized training maintains $|c_t|$ near zero, whereas asynchronous training exhibits persistently elevated alignment prior to collapse. GAC partitions the alignment space using two thresholds $0 < c_{\text{low}} < c_{\text{high}}$, corresponding to three operational regimes:

Safe regime ($|c_t| \leq c_{\text{low}}$). Alignment remains within the on-policy range. No intervention is applied and the update proceeds normally: $\theta_{t+1} = \theta_t + \eta \hat{g}_t$.

Projection regime ($c_{\text{low}} < |c_t| < c_{\text{high}}$). Alignment is elevated but correctable. GAC applies directional projection to reduce alignment to the target level c_{low} .

Violation regime ($|c_t| \geq c_{\text{high}}$). Alignment indicates a severe trust-region violation. The update is skipped to prevent destabilizing overshoot: $\theta_{t+1} = \theta_t$.

In the projection regime, GAC uses the previous gradient as

the reference direction, $u_{t-1} \triangleq \hat{g}_{t-1}/\|\hat{g}_{t-1}\|_2$, and rescales the parallel component to achieve the target alignment:

$$\hat{g}'_t = \frac{c_{\text{low}}}{|c_t|} \langle \hat{g}_t, u_{t-1} \rangle u_{t-1} + \left(\hat{g}_t - \langle \hat{g}_t, u_{t-1} \rangle u_{t-1} \right). \quad (4)$$

This rescaling preserves orthogonal gradient information while reducing the magnitude of the alignment component.

4.3. Provable Benefit

We now connect the projection mechanism to the theoretical analysis of staleness-induced bias, b_t . The following proposition formalizes how GAC attenuates this effect.

Proposition 4.1 (Bias reduction via orthogonal projection, Informal). *Assume the small-drift linearization and temporal persistence conditions hold, such that $b_t \approx \eta_{t-1} B_t \hat{g}_{t-1}$. Let b_t^\perp denote the effective bias after applying GAC with $\alpha \leq \beta$. Then*

$$\mathbb{E}\|b_t^\perp\|^2 \leq \mathbb{E}\|b_t\|^2 - \eta^2 \lambda_t^2 \mathbb{E}\|\hat{g}_{t-1}\|^2 + \mathcal{O}(\epsilon_t), \quad (5)$$

where $\lambda_t > 0$ quantifies the alignment strength between b_t and \hat{g}_{t-1} , and ϵ_t collects higher-order approximation terms.

Interpretation. The formal version of Proposition 4.1 and its proof can be found in Appendix F. Proposition 4.1 shows that suppressing the previous-step direction yields a *strict reduction* in the magnitude of the staleness-induced bias. The removed term scales with the same persistence factor λ_t that drives gradient alignment under stale rollouts. Consequently, GAC directly weakens the mechanism responsible for pre-collapse amplification, providing a principled explanation for the stabilization effects observed empirically.

5. Experiments

In this section, we conduct a comprehensive evaluation of GAC for stabilizing off-policy GRPO training induced by stale rollouts. Across experiments, GAC remains stable at large staleness, consistently outperforms off-policy baselines, and recovers on-policy-level performance. Implementation details, additional results and hyperparameter choices are provided in Appendix C.

Experimental setup. We extensively evaluate GAC on seven mathematical reasoning benchmarks: AIME24/25 (Art of Problem Solving, 2024a), AMC23/24 (Art of Problem Solving, 2024b), Math500 (Hendrycks et al., 2021), OlympiadBench (He et al., 2024), and MinervaMath (Lewkowycz et al., 2022). Experiments use widely adopted Qwen3 model family at three parameter scales (1.7B/4B/8B) (Yang et al., 2025), and Llama3.2-3B-Instruct (Grattafiori et al., 2024) to verify robustness across different architectures. We vary the staleness level over $s \in \{4, 8, 16, 32\}$ to assess performance under different degrees of asynchrony.

Baselines. We compare GAC against three off-policy baselines designed for stale-rollout optimization: **GRPO** (Shao et al., 2024), standard GRPO applied directly to stale rollouts; **M2PO** (Zheng et al., 2025), a trust-region method designed to handle large staleness; and **BAPO** (Xi et al., 2025), an adaptive clipping approach for off-policy RL. We also report **GRPO** ($s=0$), fully synchronized training with fresh rollouts, as the on-policy reference.

5.1. Training Dynamics Under Staleness

We evaluate the efficacy of GAC under large staleness ($s = 16$, which saturates throughput gains in most asynchronous RL systems) by analyzing both convergence behavior and the underlying gradient-alignment mechanism.

Convergence behavior. Figure 2 presents training reward and validation accuracy (from MinervaMath (Lewkowycz et al., 2022) for Qwen3-1.7B/4B/8B and Llama-3.2-3B-Instruct. All off-policy baselines exhibit unstable convergence across model scales: reward and accuracy undergo severe fluctuations, abrupt drops, and in extreme cases, complete collapse. In contrast, GAC maintains smooth monotonic convergence throughout training, achieving stability comparable to synchronized GRPO. Critically, GAC achieves this stability without sacrificing sample efficiency, converging at rates comparable to synchronized training without requiring extended optimization and reaching similar final performance. The consistent behavior across the 1.7B–8B range and both model families demonstrates that explicit alignment control resolves the fundamental instability of asynchronous GRPO.

Gradient alignment regulation. Figure 3 reports the consecutive-gradient cosine similarity c_t for Qwen3-4B and Qwen3-8B, revealing the mechanism behind GAC’s stabilization. Synchronized training (GRPO, $s=0$) and GAC both keep $|c_t|$ tightly concentrated near zero with negligible variance throughout optimization, indicating near-orthogonal consecutive gradients. In contrast, the off-policy baselines—stale-rollout GRPO, M2PO and BAPO—exhibit a sustained rise in $|c_t|$ that escalates to high magnitudes with severe oscillations. GAC restores gradient-alignment dynamics to the same low-alignment regime observed in synchronized training, consistent with its intended mechanism of regulating update geometry under staleness.

5.2. Model Performance

Table 1 summarizes accuracy on seven reasoning benchmarks under a large staleness setting ($s=16$), with synchronized GRPO ($s=0$) reported as an on-policy reference. Across model families and scales, stale-rollout GRPO and strong off-policy baselines (M2PO, BAPO) exhibit substantial accuracy degradation under staleness, consistently un-

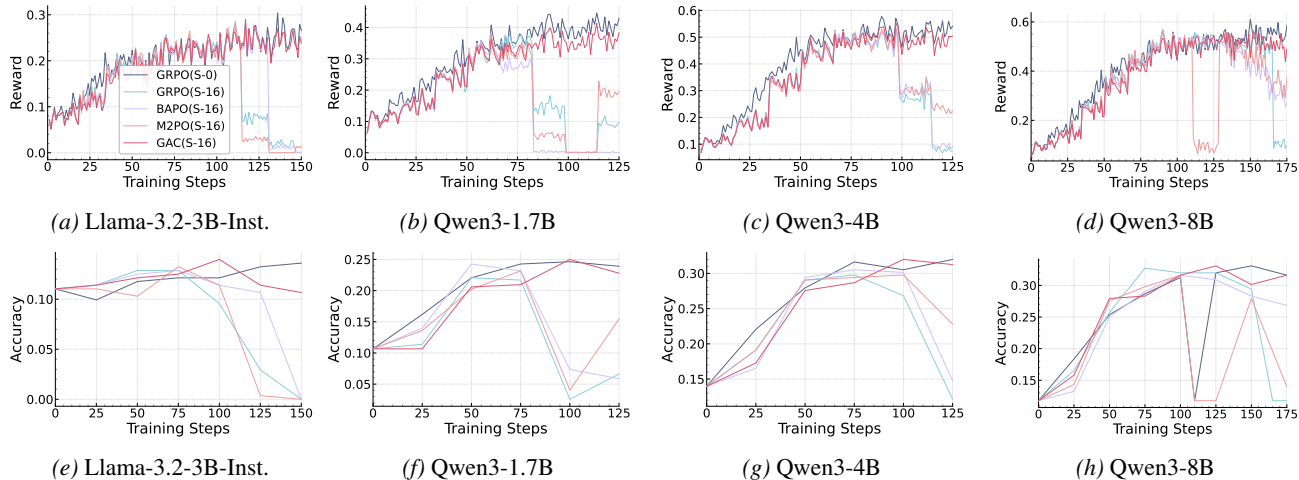


Figure 2. **Cross-scale learning curves under large staleness.** Panels (a–d) report training reward and panels (e–h) report MinervaMath validation accuracy for Qwen3-1.7B/4B/8B and Llama-3.2-3B-Instruct. Curves compare synchronized GRPO, stale-rollout GRPO, M2PO, BAPO, and GAC.

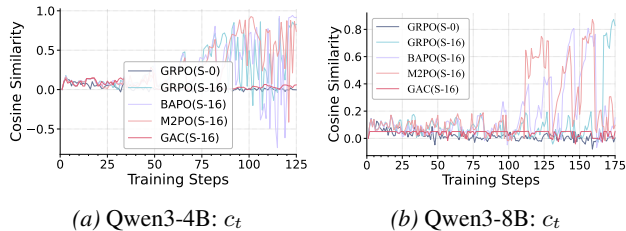


Figure 3. **Gradient-alignment dynamics under staleness.** Consecutive-gradient cosine similarity c_t for Qwen3-4B/8B, comparing synchronized GRPO, stale-rollout GRPO, M2PO, BAPO and GAC.

derperforming the on-policy reference. This persistent gap underscores the fundamental challenge of maintaining stable optimization under asynchrony. In contrast, GAC achieves the highest average accuracy among stale-rollout methods and largely closes the gap to synchronized training. On Qwen3-8B, GAC achieves 50.2% compared to 51.0% for the on-policy reference, while off-policy baselines fall 4–5 points below. The gap between GAC and off-policy baselines is most pronounced on challenging benchmarks, where staleness-induced degradation is amplified. For instance, on AIME24/25 with Qwen3-4B, GAC attains 30.2/30.0, essentially matching synchronized training (30.1/30.2), while off-policy baselines degrade substantially.

5.3. Ablations

Robustness to varying staleness. We extend our analysis to $s \in \{4, 8, 16, 32\}$ to assess generalization across asynchrony regimes. Figure 4 shows that GAC maintains stable convergence across all staleness levels, including $s=32$ where stale-rollout GRPO collapses entirely. In contrast to the progressive degradation of stale-rollout GRPO observed in Section 3.1, GAC achieves stable performance across the entire staleness range.

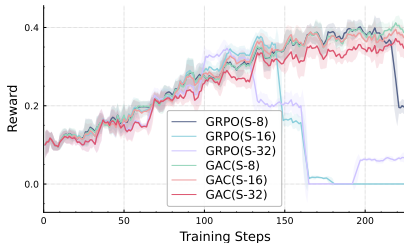


Figure 4. **Robustness across staleness levels.** Training reward trajectories comparing stale-rollout GRPO and GAC under $s \in \{8, 16, 32\}$. GAC maintains stable convergence across staleness levels, whereas stale-rollout GRPO degrades progressively as staleness increases.

6. Related Work

Due to space limitations, we focus on the most directly related work in the main text and defer a more detailed discussion to Appendix B.

As reinforcement learning workloads scale, end-to-end training is increasingly constrained by heterogeneous pipeline stages, where rollout generation and reward evaluation often dominate wall-clock time. A widely adopted systems solution is to use disaggregated actor–learner architectures that decouple trajectory collection from optimization, thereby improving throughput and mitigating straggler effects. Early asynchronous methods such as A3C (Mnih et al., 2016) demonstrated that relaxing strict synchronization can substantially improve scalability, while IMPALA (Espeholt et al., 2018) introduced importance-corrected actor–learner updates (via V-trace) to control off-policy drift at scale. Subsequent systems refined this paradigm through more aggressive data reuse and communication-efficient designs, including Ape-X (Horgan et al., 2018) and SEED RL (Espeholt et al., 2020). Collectively, these works establish asynchrony and staleness as practical ingredients for high-throughput

Table 1. Accuracy under Staleness. Accuracy (%) on seven mathematical reasoning benchmarks for Qwen3 models (1.7B/4B/8B) and Llama-3.2-3B-Instruct. We report synchronized on-policy GRPO (GRPO-Sync, $s=0$) as a *reference* (shaded rows). All other methods are evaluated under stale-rollout training with $s=16$. **Avg.** denotes the mean accuracy across benchmarks. **Bold** marks the best average accuracy among stale-rollout methods for each model. The last column reports Δ_{Avg} , computed as the improvement of GAC over the strongest stale-rollout baseline among {GRPO, M2PO, BAPO} for the same model.

Method	AIME24	AIME25	AMC23	AMC24	Math500	Miner.	Olymp.	Avg.	Δ_{Avg}
<i>Llama-3.2-3B-Instruct</i>									
GRPO-Sync	16.7	3.3	28.3	15.6	48.4	13.6	14.6	20.1	–
GRPO	10.0	3.0	27.5	13.1	48.8	12.8	14.3	18.5	–
M2PO	13.3	2.9	27.9	13.3	48.3	13.2	13.2	18.9	–
BAPO	6.7	2.9	25.7	15.4	49.2	12.9	14.0	18.1	–
GAC	16.6	3.2	32.5	15.8	47.8	14.0	13.8	20.5	+1.6
<i>Qwen3-1.7B</i>									
GRPO-Sync	16.7	16.9	55.0	53.3	75.4	25.0	28.4	38.7	–
GRPO	10.0	13.3	47.5	44.4	68.6	22.1	25.7	33.1	–
M2PO	13.3	13.6	42.5	40.2	72.4	23.2	24.1	32.7	–
BAPO	16.8	10.2	47.5	38.6	68.4	24.2	24.3	32.8	–
GAC	20.0	16.8	54.1	48.9	73.6	25.1	28.1	38.1	+5.0
<i>Qwen3-4B</i>									
GRPO-Sync	30.1	30.2	77.6	68.9	84.6	34.2	36.2	51.7	–
GRPO	24.2	23.3	70.3	62.2	77.8	29.6	32.9	45.8	–
M2PO	26.7	20.2	71.1	62.8	78.4	29.9	33.4	46.1	–
BAPO	26.8	20.1	75.0	60.3	80.2	30.5	33.9	46.7	–
GAC	30.2	30.0	80.1	64.5	83.7	32.5	34.9	50.8	+4.1
<i>Qwen3-8B</i>									
GRPO-Sync	26.7	26.6	85.0	66.7	83.0	33.1	36.2	51.0	–
GRPO	23.3	23.1	72.3	62.2	82.2	32.7	33.9	47.1	–
M2PO	23.5	20.2	72.5	60.0	82.4	31.8	33.2	46.2	–
BAPO	26.8	23.4	65.2	66.4	81.9	31.6	32.6	46.8	–
GAC	30.0	26.4	78.5	66.5	82.5	33.0	34.4	50.2	+3.1

RL, while also highlighting that delayed gradients and stale rollouts can fundamentally alter optimization behavior and introduce additional instability.

Motivated by similar efficiency bottlenecks in large language model post-training, recent work revisits asynchronous execution for RLHF and RLVR under expensive inference-time rollouts. Asynchronous RLHF formulations explicitly exploit off-policy data reuse to improve throughput (Noukhovitch et al., 2024), while large-scale LLM-RL infrastructures such as AReL (Fu et al., 2025) and AsyncFlow (Han et al., 2025) support decoupled rollout and optimization for scalable reasoning post-training. However, this decoupling naturally introduces stale-rollout gradients, where updates are computed using trajectories generated by lagged behavior policies. Under large staleness, this effect amplifies distribution mismatch and destabilizes GRPO-style optimization. Recent off-policy stabilization methods for LLM-RL, such as M2PO (Zheng et al., 2025) and BAPO (Xi et al., 2025), primarily address this issue by strengthening GRPO-style trust-region surrogates through adaptive clipping or likelihood-ratio shaping.

In contrast, our method operates at the optimizer interface and is complementary to these approaches. Rather than

modifying surrogate objectives or correcting distributional shift, we directly regulate the geometry of the aggregated policy update by suppressing progress along stale-aligned directions. This provides a lightweight, system-agnostic stabilization mechanism that targets the alignment-driven instability induced by asynchronous execution.

7. Conclusion

This paper studies asynchronous GRPO from a training-dynamics perspective and demonstrates that asynchrony can fundamentally alter training dynamics, leading to collapse. Through both empirical evidence and theoretical analysis, we identify persistently elevated consecutive-gradient cosine similarity as a reliable precursor to training collapse, capturing the accumulation of stale-aligned updates. Motivated by this insight, we propose GAC, a lightweight gradient-space controller that stabilizes asynchronous GRPO by explicitly regulating progress along stale-aligned directions while preserving informative residual updates. GAC operates at the optimizer interface, is system- and algorithm-agnostic, and incurs only constant per-step overhead. Our results demonstrate that GAC effectively stabilizes asynchronous GRPO and restores robust training dynamics under staleness.

Impact Statement

This paper presents work whose goal is to advance the training of reinforcement learning. There are many potential societal consequences of our work, none of which we feel must be specifically highlighted here.

References

- Art of Problem Solving. AIME Problems and Solutions. <https://artofproblemsolving.com/wiki/index.php/AIME>, 2024a. Accessed: 2026-01-28.
- Art of Problem Solving. AMC Problems and Solutions. <https://artofproblemsolving.com/wiki/index.php/AMC>, 2024b. Accessed: 2026-01-28.
- Bai, Y., Jones, A., Ndousse, K., Askell, A., Chen, A., DasSarma, N., Drain, D., Fort, S., Ganguli, D., et al. Training a helpful and harmless assistant with reinforcement learning from human feedback. *arXiv preprint arXiv:2204.05862*, 2022.
- DeepSeek-AI. DeepSeek-R1: Incentivizing reasoning capability in LLMs via reinforcement learning. *arXiv preprint arXiv:2501.12948*, 2025. URL <https://arxiv.org/abs/2501.12948>.
- Espeholt, L., Soyer, H., Munos, R., Simonyan, K., Mnih, V., Ward, T., Doron, Y., Firoiu, V., Harley, T., Dunning, I., Legg, S., and Kavukcuoglu, K. IMPALA: Scalable distributed deep-RL with importance weighted actor-learner architectures. In Dy, J. and Krause, A. (eds.), *Proceedings of the 35th International Conference on Machine Learning*, volume 80 of *Proceedings of Machine Learning Research*, pp. 1407–1416. PMLR, 10–15 Jul 2018.
- Espeholt, L., Marinier, R., Stańczyk, P., Wang, K., and Michalski, M. Seed rl: Scalable and efficient deep-rl with accelerated central inference. In *International Conference on Learning Representations (ICLR)*, 2020.
- Feng, L., Xue, Z., Liu, T., and An, B. Group-in-group policy optimization for llm agent training. *arXiv preprint arXiv:2505.10978*, 2025.
- Fu, W., Gao, J., Shen, X., Zhu, C., Mei, Z., He, C., Xu, S., Wei, G., Mei, J., Wang, J., Yang, T., Yuan, B., and Wu, Y. Areal: A large-scale asynchronous reinforcement learning system for language reasoning. *arXiv preprint arXiv:2505.24298*, 2025.
- Gao, C., Zheng, C., Chen, X.-H., Dang, K., Liu, S., Yu, B., Yang, A., Bai, S., Zhou, J., and Lin, J. Soft adaptive policy optimization. *arXiv preprint arXiv:2501.20347*, 2025. Qwen Team, Alibaba.
- Grattafiori, A., Dubey, A., Jauhri, A., Pandey, A., Kadian, A., Al-Dahle, A., Letman, A., Mathur, A., Schelten, A., Fan, A., et al. The llama 3 herd of models. *arXiv preprint arXiv:2407.21783*, 2024.
- Han, Z., You, A., Wang, H., Luo, K., Yang, G., Shi, W., Chen, M., Zhang, S., Lan, Z., Deng, C., Ji, H., Liu, W., Huang, Y., Zhang, Y., Pan, C., Wang, J., Huang, X., Li, C., and Wu, J. Asyncflow: An asynchronous streaming rl framework for efficient llm post-training. *arXiv preprint arXiv:2507.01663*, 2025.
- He, C., Luo, R., Bai, Y., Hu, S., Thai, Z. L., Shen, J., Hu, J., Han, X., Huang, Y., Zhang, Y., et al. Olympiad-bench: A challenging benchmark for promoting AGI with olympiad-level bilingual multimodal scientific problems. *arXiv preprint arXiv:2402.14008*, 2024.
- Hendrycks, D., Burns, C., Kadavath, S., Arora, A., Basart, S., Tang, E., Song, D., and Steinhardt, J. Measuring mathematical problem solving with the MATH dataset. *arXiv preprint arXiv:2103.03874*, 2021.
- Horgan, D., Quan, J., Budden, D., Barth-Maron, G., Hessel, M., van Hasselt, H., and Silver, D. Distributed prioritized experience replay. In *International Conference on Learning Representations (ICLR)*, 2018.
- Le, T., Bui, N. D., Ngo Van, L., and Le, T. Sharpness-controlled group relative policy optimization with token-level probability shaping. *arXiv preprint arXiv:2511.00066*, 2025.
- Lewkowycz, A., Andreassen, A., Dohan, D., Dyer, E., Michalewski, H., Ramasesh, V., Slone, A., Anil, C., Schlag, I., Gutman-Solo, T., et al. Solving quantitative reasoning problems with language models. In *Advances in Neural Information Processing Systems*, volume 35, pp. 3843–3857, 2022.
- Li, X., Wu, S., and Shen, Z. A-3po: Accelerating asynchronous llm training with staleness-aware proximal policy approximation, 2026.
- Lightman, H., Kosaraju, V., Burda, Y., Edwards, H., Baker, B., Lee, T., Leike, J., Schulman, J., Sutskever, I., and Cobbe, K. Let’s verify step by step. *arXiv preprint arXiv:2305.20050*, 2023.
- Lu, H., Liu, Z., Xiong, S., He, Y., Gao, W., Wu, Y., Wang, W., Liu, J., Li, Y., Zhao, H., Huang, J., Yang, S., Li, X., Luo, Y., Liu, Z., Pan, L., Yan, J., Wang, W., Su, W., Wang, J., Qu, L., and Zheng, B. Part ii: Roll flash – accelerating rlvr and agentic training with asynchrony, 2025.
- Mnih, V., Badia, A. P., Mirza, M., Graves, A., Lillicrap, T., Harley, T., Silver, D., and Kavukcuoglu, K. Asynchronous methods for deep reinforcement learning. In *International Conference on Machine Learning*, 2016.

- Noukhovitch, M., Huang, S., Xhonneux, S., Hosseini, A., Agarwal, R., and Courville, A. Asynchronous RLHF: Faster and more efficient off-policy RL for language models. *arXiv preprint arXiv:2410.18252*, 2024.
- Ouyang, L., Wu, J., Jiang, X., Almeida, D., Wainwright, C., Mishkin, P., Zhang, C., Agarwal, S., Slama, K., Ray, A., et al. Training language models to follow instructions with human feedback. *arXiv preprint arXiv:2203.02155*, 2022.
- Schulman, J., Levine, S., Moritz, P., Jordan, M. I., and Abbeel, P. Trust region policy optimization. *arXiv preprint arXiv:1502.05477*, 2015.
- Schulman, J., Wolski, F., Dhariwal, P., Radford, A., and Klimov, O. Proximal policy optimization algorithms. In *arXiv preprint arXiv:1707.06347*, 2017.
- Shao, Z., Wang, P., Zhu, Q., Xu, R., Song, J., Bi, X., Zhang, H., Zhang, M., Li, Y. K., Wu, Y., et al. Deepseekmath: Pushing the limits of mathematical reasoning in open language models. *arXiv preprint arXiv:2402.03300*, 2024.
- Sheng, G., Zhang, C., Ye, Z., Wu, X., Zhang, W., Zhang, R., Peng, Y., Lin, H., and Wu, C. Hybridflow: A flexible and efficient rlhf framework, 2024.
- Sheng, G., Tong, Y., Wan, B., Zhang, W., Jia, C., Wu, X., Wu, Y., Li, X., Zhang, C., Peng, Y., Lin, H., Liu, X., and Wu, C. Laminar: A scalable asynchronous rl post-training framework, 2025.
- Uesato, J., Kushman, N., Kumar, R., Song, F., Siegel, N., Wang, L., Creswell, A., Irving, G., and Higgins, I. Solving math word problems with process-and outcome-based feedback. *arXiv preprint arXiv:2211.14275*, 2022.
- Wang, S., Zhang, S., Zhang, J., Hu, R., Li, X., Zhang, T., Li, J., Wu, F., Wang, G., and Hovy, E. Reinforcement learning enhanced llms: A survey, 2025a.
- Wang, W., Xiong, S., Chen, G., Gao, W., Guo, S., He, Y., Huang, J., Liu, J., Li, Z., Li, X., et al. Reinforcement learning optimization for large-scale learning: An efficient and user-friendly scaling library. *arXiv preprint arXiv:2506.06122*, 2025b.
- Wen, L., Cai, Y., Xiao, F., He, X., An, Q., Duan, Z., Du, Y., Liu, J., Tang, L., Lv, X., Zou, H., Deng, Y., Jia, S., and Zhang, X. Light-rl: Curriculum sft, dpo and rl for long cot from scratch and beyond. *arXiv preprint arXiv:2503.10460*, 2025.
- Xi, Z., Guo, X., Nan, Y., Zhou, E., Shen, J., Chen, W., Liu, J., Huang, J., Zhang, Z., Guo, H., Deng, X., Lei, Z., Zheng, M., Wang, G., Zhang, S., Sun, P., Zheng, R., Yan, H., Gui, T., Zhang, Q., and Huang, X. Bapo: Stabilizing off-policy reinforcement learning for llms via balanced policy optimization with adaptive clipping, 2025.
- Yang, A., Li, A., Yang, B., Zhang, B., Hui, B., Zheng, B., Yu, B., Gao, C., Huang, C., Lv, C., et al. Qwen3 technical report. *arXiv preprint arXiv:2505.09388*, 2025.
- Yu, Z. et al. Dapo: An open-source llm reinforcement learning system at scale. *arXiv preprint arXiv:2503.14476*, 2025.
- Zhang, K., Zuo, Y., He, B., Sun, Y., Liu, R., Jiang, C., Fan, Y., Tian, K., Jia, G., Li, P., Fu, Y., Lv, X., Zhang, Y., Zeng, S., Qu, S., Li, H., Wang, S., Wang, Y., Long, X., Liu, F., Xu, X., Ma, J., Zhu, X., Hua, E., Liu, Y., Li, Z., Chen, H., Qu, X., Li, Y., Chen, W., Yuan, Z., Gao, J., Li, D., Ma, Z., Cui, G., Liu, Z., Qi, B., Ding, N., and Zhou, B. A survey of reinforcement learning for large reasoning models, 2025.
- Zheng, C., Liu, S., Li, M., Chen, X.-H., Yu, B., Gao, C., Dang, K., Liu, Y., Men, R., Yang, A., Zhou, J., and Lin, J. Group sequence policy optimization. *arXiv preprint arXiv:2412.15498*, 2024. Qwen Team, Alibaba.
- Zheng, H., Zhao, J., and Chen, B. Prosperity before collapse: How far can off-policy rl reach with stale data on llms?, 2025.
- Zhong, Y., Zhang, Z., Song, X., Hu, H., Jin, C., Wu, B., Chen, N., Chen, Y., Zhou, Y., Wan, C., Zhou, H., Jiang, Y., Zhu, Y., and Jiang, D. Streamrl: Scalable, heterogeneous, and elastic rl for llms with disaggregated stream generation, 2025.
- Ziegler, D. M., Stiennon, N., Wu, J., Brown, T. B., Radford, A., Amodei, D., Christiano, P. F., and Irving, G. Fine-tuning language models from human preferences. *arXiv preprint arXiv:1909.08593*, 2019.

A. Additional Details and Discussion

A.1. Computing Consecutive-Gradient Cosine Similarity

We provide implementation details for the consecutive-gradient cosine similarity c_t in Eq. (1). At update step t , we define \hat{g}_t as the aggregated policy gradient *estimate* after completing backpropagation and gradient accumulation for the GRPO objective (using the rollout data available at step t , which may be stale). We conceptually treat \hat{g}_t as the flattened concatenation of all trainable parameter gradients. The metric c_t is scale-invariant and serves as a geometric diagnostic of successive update directions.

Efficient computation under data parallelism. Under distributed training with gradient sharding (e.g., FSDP, DeepSpeed ZeRO), we compute c_t without materializing full gradients. Let $\hat{g}_t^{(r)}$ and $\hat{g}_{t-1}^{(r)}$ denote gradient shards on rank r . Each rank computes three local dot products:

$$\langle \hat{g}_t^{(r)}, \hat{g}_{t-1}^{(r)} \rangle, \quad \langle \hat{g}_t^{(r)}, \hat{g}_t^{(r)} \rangle, \quad \langle \hat{g}_{t-1}^{(r)}, \hat{g}_{t-1}^{(r)} \rangle, \quad (6)$$

followed by a single all-reduce to obtain global quantities

$$\langle \hat{g}_t, \hat{g}_{t-1} \rangle, \quad \|\hat{g}_t\|_2^2, \quad \|\hat{g}_{t-1}\|_2^2. \quad (7)$$

We then compute

$$c_t = \frac{\langle \hat{g}_t, \hat{g}_{t-1} \rangle}{\sqrt{\|\hat{g}_t\|_2^2 \cdot \|\hat{g}_{t-1}\|_2^2 + \epsilon}}, \quad (8)$$

where $\epsilon = 10^{-8}$ ensures numerical stability.

Evaluation protocol. Unless otherwise stated, c_t is computed on raw aggregated gradient estimates \hat{g}_t before optimizer transformations or GAC intervention.

A.2. Computational and Memory Overhead

Computational overhead. GAC introduces only lightweight overhead beyond standard gradient computation. Per update, it evaluates the consecutive-gradient cosine similarity c_t using a constant number of inner products on sharded gradients and a constant-size collective reduction to aggregate the required statistics across workers. Under distributed training with gradient sharding (e.g., FSDP or DeepSpeed ZeRO), this adds negligible communication volume relative to routine training collectives, with overhead primarily arising from an additional synchronization point.

When $|c_t|$ falls in the projection regime ($c_{\text{low}} < |c_t| < c_{\text{high}}$), GAC applies an adaptive rank-one correction to the current gradient:

$$\hat{g}'_t = \beta \hat{g}_t + (\alpha - \beta) \langle \hat{g}_t, u_{t-1} \rangle u_{t-1}, \quad (9)$$

where $\alpha = c_{\text{low}}/|c_t|$ is computed dynamically and we use $\beta = 1$. This intervention consists of a small number of elementwise linear operations (a scale and an addition) and therefore incurs $O(d_{\text{local}})$ memory-bandwidth work per update, where d_{local} is the number of gradient elements on the local rank. The projection is applied in-place to parameter gradients and does not require additional forward/backward passes.

Memory footprint. GAC maintains a single additional gradient snapshot for the previous update direction \hat{g}_{t-1} , resulting in an $O(d_{\text{local}})$ persistent memory overhead per rank. Any temporary buffers used to flatten gradients for similarity computation are short-lived and do not affect the asymptotic memory complexity.

A.3. Pseudocode for GAC

Algorithm 1 provides the complete pseudocode of GAC. At each update, GAC computes the consecutive-gradient cosine similarity c_t and selects among three behaviors: a standard gradient step in the low-alignment regime, an adaptive projection step that suppresses the component aligned with the previous gradient, or an update skip when alignment exceeds the high-threshold safeguard.

Algorithm 1 Gradient Alignment Control (GAC)

```

1: Input: thresholds  $c_{\text{low}}, c_{\text{high}}$ , learning rate  $\eta$ 
2: Initialize:  $\theta_0, \hat{g}_0 \leftarrow 0$ 
3: for  $t = 1, 2, \dots, T$  do
4:   Compute gradient  $\hat{g}_t$  from stale rollouts under  $\pi_{\theta_{t-\tau}}$ 
5:    $c_t \leftarrow \langle \hat{g}_t, \hat{g}_{t-1} \rangle / (\|\hat{g}_t\|_2 \|\hat{g}_{t-1}\|_2)$ 
6:   if  $|c_t| \leq c_{\text{low}}$  then
7:      $\theta_t \leftarrow \theta_{t-1} + \eta \hat{g}_t$ 
8:   else if  $|c_t| \geq c_{\text{high}}$  then
9:      $\theta_t \leftarrow \theta_{t-1}$ 
10:  else
11:     $u \leftarrow \hat{g}_{t-1} / \|\hat{g}_{t-1}\|_2, \quad \alpha \leftarrow c_{\text{low}} / |c_t|$ 
12:     $g_{\parallel} \leftarrow \langle \hat{g}_t, u \rangle u, \quad g_{\perp} \leftarrow \hat{g}_t - g_{\parallel}$ 
13:     $\hat{g}'_t \leftarrow \alpha g_{\parallel} + g_{\perp}$ 
14:     $\theta_t \leftarrow \theta_{t-1} + \eta \hat{g}'_t$ 
15:  end if
16: end for

```

B. Extended Related Work

RLVR and GRPO Variants. Reinforcement learning has become a standard paradigm for post-training large language models toward complex objectives. Algorithmically, modern RL for LLMs largely builds upon trust-region policy optimization, from TRPO (Schulman et al., 2015) to PPO (Schulman et al., 2017), which stabilizes updates via constrained or clipped surrogate objectives. These foundations enabled RLHF to achieve strong empirical gains in summarization, instruction following, and safety alignment (Ziegler et al., 2019; Ouyang et al., 2022; Bai et al., 2022). More recently, reinforcement learning with verifiable rewards (RLVR) has gained prominence in reasoning-centric post-training, substituting learned reward models with programmatic verifiers that yield sparse, binary feedback (Lightman et al., 2023; Uesato et al., 2022). This paradigm shift necessitates optimization methods robust to high-variance, outcome-level signals. GRPO (Shao et al., 2024; DeepSeek-AI, 2025) has emerged as a canonical RLVR algorithm, inspiring a growing family of variants designed to enhance stability and credit assignment under verifier sparsity. Notable examples include DAPO (Yu et al., 2025), which decouples clipping design from sampling allocation to prioritize informative rollouts; GSPO (Zheng et al., 2024), which applies sequence-level rather than token-level trust-region control; SAPO (Gao et al., 2025), which adapts clipping thresholds dynamically to improve stability-exploration tradeoffs; and TR-GRPO (Le et al., 2025), which introduces token-aware modifications for robust credit assignment. Beyond surrogate-level redesigns, Light-R1 (Wen et al., 2025) demonstrates a practical post-training pipeline for long-CoT reasoning in which GRPO is employed as the RL stage on long-CoT models, further improving mathematical reasoning performance. While these methods primarily improve GRPO via surrogate-level redesigns, we take an optimizer-level perspective that stabilizes the policy update by directly controlling its geometry.

Asynchronous RL Training Frameworks and Off-policy RL Algorithms. As RL workloads scale, end-to-end training is increasingly constrained by heterogeneous pipeline stages, where rollout generation and reward evaluation often dominate wall-clock time. A common systems solution is to adopt disaggregated actor–learner architectures that decouple trajectory collection from optimization, thereby improving throughput and mitigating straggler effects. Early asynchronous methods such as A3C (Mnih et al., 2016) demonstrated that relaxing strict synchronization can substantially improve scalability, while IMPALA (Espeholt et al., 2018) introduced an importance-corrected actor–learner design (via V-trace) to control off-policy drift at scale. Subsequent systems further refined the same principle through more aggressive data reuse and communication efficiency, including replay-centric distributed training in Ape-X (Horgan et al., 2018) and accelerated centralized inference in SEED RL (Espeholt et al., 2020). Collectively, these works establish asynchrony and staleness as practical ingredients for high-throughput RL, while also underscoring that delayed gradients and stale rollouts can introduce nontrivial off-policy effects that may require additional stabilization when instantiated in GRPO-style LLM post-training.

Motivated by similar efficiency bottlenecks in LLM post-training, recent work revisits asynchronous execution for RLHF and RLVR under expensive inference-time rollouts. For example, asynchronous RLHF formulations explicitly exploit off-policy data reuse to improve throughput (Noukhovitch et al., 2024), while large-scale LLM-RL infrastructures such as AReaL (Fu et al., 2025) and AsyncFlow (Han et al., 2025) support decoupled rollout–train execution for scalable reasoning post-training.

Table 2. GRPO hyperparameters. Configuration used across all experiments.

Parameter	Value
<i>Optimization</i>	
Optimizer	AdamW
Learning rate (η)	1×10^{-6}
AdamW β 's	(0.9, 0.999)
AdamW ϵ_{adam}	1×10^{-8}
Weight decay	1×10^{-2}
Clip ratio (ϵ_{clip})	0.2
Entropy coefficient	0.001
KL coefficient	0.001
KL loss type	low_var_kl
Gradient clipping	True
<i>Training</i>	
Train batch size	256
Responses per prompt (n)	8
Critic warmup steps	0
Evaluation frequency	25
<i>Generation</i>	
Sampling	True
Temperature	0.6
Top- p	0.95
Max sequence length	2048

However, this decoupling naturally introduces *stale-rollout gradients*, where updates are computed on trajectories generated by lagged behavior policies, amplifying distribution mismatch and destabilizing GRPO-style optimization under large staleness. To address this challenge, recent off-policy stabilization methods for LLM-RL, such as M2PO (Zheng et al., 2025) and BAPO (Xi et al., 2025), primarily reinforce GRPO-style trust-region surrogates through adaptive clipping and likelihood-ratio shaping, which improves robustness under stale data. In contrast, our method is complementary and operates at the optimizer interface: we directly regulate the geometry of the aggregated update by suppressing progress along stale-aligned directions, providing a lightweight, system-agnostic stabilization layer for asynchronous RL pipelines.

C. Implementation Details

C.1. Testbed

All experiments are conducted on a single 8-GPU machine equipped with NVIDIA H800-80GB GPUs, interconnected via 400 GB/s NVLink. Our software stack uses CUDA 12.6, PyTorch 2.7.1, NCCL 2.26.2, vLLM 0.10.0, and FlashAttention 2.7.4.post1.

C.2. Training framework

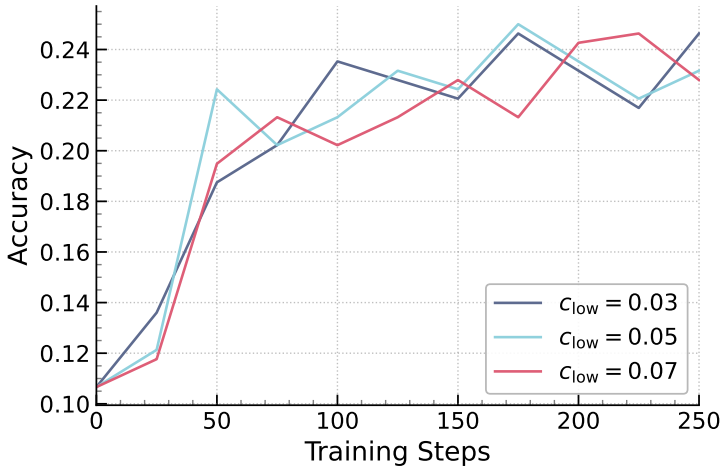
All experiments are implemented on top of the open-source VERL (Sheng et al., 2024) framework, which provides an end-to-end RL post-training pipeline for large language models. VERL couples rollout generation with policy optimization in a modular design, enabling both fully synchronized execution and stale-rollout (asynchronous) training within the same codebase.

C.3. Hyperparameters

Common hyperparameters. We use a single shared GRPO training recipe across all methods and model scales to ensure controlled comparisons. In particular, we fix the learning rate to 1×10^{-6} and the train batch size to 256 in all experiments. Unless otherwise stated, the remaining optimization and generation settings are also kept identical, including the clipping threshold, entropy/KL regularization, and decoding parameters. Table 2 summarizes the full set of common hyperparameters.

Table 3. **On-policy ($s=0$) statistics of consecutive-gradient alignment.** We report the 90th percentile $q_{0.9}(|c_t|)$, the maximum $\max |c_t|$, and the fraction of updates with $|c_t| \leq 0.05$ (computed over updates after step 50 to exclude early transients). These values motivate anchoring c_{low} to the on-policy range and setting c_{high} well above it.

Model	$q_{0.9}(c_t)$	$\max c_t $	$\Pr(c_t \leq 0.05)$
Qwen3-1.7B	0.0471	0.0924	0.91
Llama-3.2-3B-Instruct	0.0687	0.1276	0.83
Qwen3-4B	0.0296	0.0645	0.99
Qwen3-8B	0.0317	0.0625	0.98



(a) **Fixed $c_{\text{high}}=0.3$.** OlympiadBench validation accuracy trajectories under $s=16$ for Qwen3-1.7B while sweeping c_{low} .

	$c_{\text{high}}=0.2$	$c_{\text{high}}=0.3$	$c_{\text{high}}=0.4$
$c_{\text{low}}=0.03$	26.8	26.3	25.5
$c_{\text{low}}=0.05$	26.2	26.9	27.1
$c_{\text{low}}=0.07$	25.7	26.6	24.9

(b) **Grid sensitivity.** Validation accuracy on OlympiadBench (Qwen3-1.7B, $s=16$) across $(c_{\text{low}}, c_{\text{high}})$; the default is highlighted.

Figure 5. **Threshold robustness of GAC.** Ablations around the default $(c_{\text{low}}, c_{\text{high}})=(0.05, 0.3)$ show that accuracy varies only mildly across nearby settings, supporting practical robustness without per-model retuning.

GAC thresholds. GAC introduces two alignment thresholds, c_{low} and c_{high} , which partition the observed consecutive-gradient cosine similarity c_t into the three operational regimes described in Section 4.2. Unless otherwise stated, we use a single default configuration across all experiments, setting $c_{\text{low}} = 0.05$ and $c_{\text{high}} = 0.3$ for both Qwen3 and Llama models and across scales. For numerical stability when computing c_t , we use $\epsilon = 10^{-8}$ in the cosine denominator.

Rationale for choosing c_{low} and c_{high} . We choose the default thresholds to be interpretable and transferable across model families and scales. The lower threshold c_{low} is anchored to the empirical on-policy alignment range measured under synchronized GRPO ($s=0$). Table 3 summarizes on-policy statistics of $|c_t|$ (computed after step 50 to exclude early transients), showing consistently small inter-step alignment across models and scales. Setting $c_{\text{low}} = 0.05$ thus places typical on-policy updates within the low-alignment regime, providing a principled reference level without per-model tuning. The upper threshold c_{high} specifies a conservative boundary for extreme alignment events; we set $c_{\text{high}} = 0.3$ to be well separated from the on-policy range (Table 3), providing a safeguard under large staleness.

Threshold robustness. Table 5b reports a local 3×3 sweep around $(c_{\text{low}}, c_{\text{high}}) = (0.05, 0.3)$. Performance remains robust across the grid, indicating that GAC is robust to threshold choice; we thus use $(0.05, 0.3)$ unchanged in all main experiments.

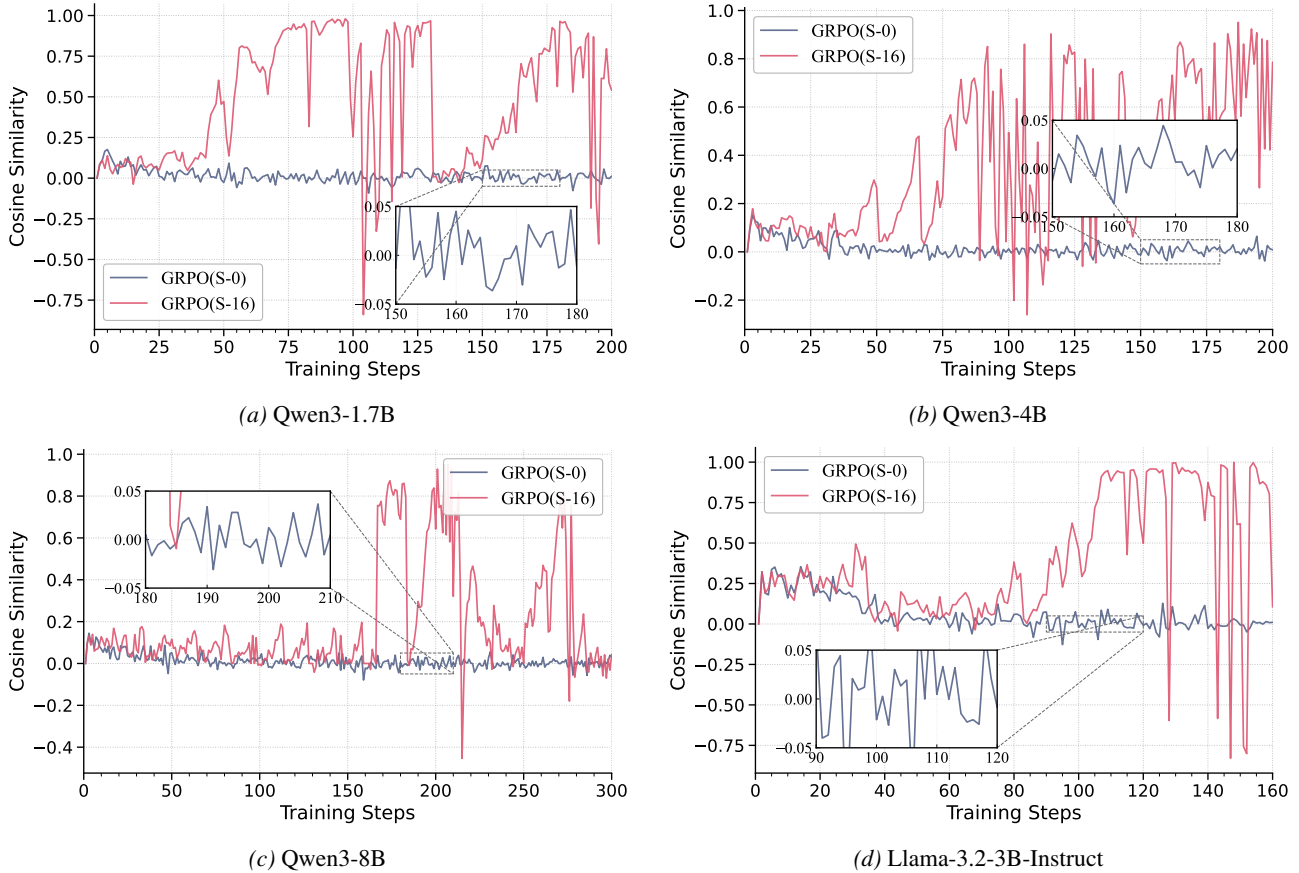


Figure 6. Consecutive-gradient cosine similarity under synchronized vs. stale-rollout training across scales. Each panel corresponds to a different model and overlays c_t for synchronized training ($s=0$) and stale-rollout training ($s=16$).

D. On-Policy Gradient Alignment Across Model Scales

Figure 6 demonstrates that synchronized GRPO maintains low consecutive-gradient alignment across model families and scales. Across all four models, on-policy training ($s=0$) keeps $|c_t|$ near zero throughout optimization, indicating near-orthogonal consecutive gradients and stable descent. Asynchronous training ($s=16$) exhibits substantially higher and more volatile $|c_t|$, consistent with the alignment-driven instability characterized in Section 3.

This gradient-geometry perspective constitutes a key contribution of our work. Existing analyses of asynchronous RL typically diagnose instability through distributional mismatch or surrogate-level trust-region violations (e.g., elevated clip fraction). We show that consecutive-gradient cosine similarity provides a direct, early indicator of training stability that precedes these conventional diagnostics, enabling proactive intervention before performance degradation occurs.

E. Formal Convergence Analysis for Asynchronous GRPO

E.1. Setup

Let L denote a differentiable surrogate objective to be *maximized*. Consider the asynchronous (stale-rollout) stochastic gradient ascent iteration

$$\theta_{t+1} = \theta_t + \eta \hat{g}_t, \tag{10}$$

where \hat{g}_t is a stochastic gradient estimator constructed from rollouts generated by a possibly stale behavior policy (e.g., $\pi_{\theta_{t-\tau_t}}$).

Throughout, we use the standard decomposition

$$\hat{g}_t = \nabla L(\theta_t) + b_t + \xi_t, \tag{11}$$

where b_t denotes the staleness-induced bias and ξ_t is a zero-mean noise term.

E.2. Assumptions

Assumption A.1 (Smoothness). L is L -smooth: for all $\theta, \theta' \in \mathbb{R}^d$,

$$\|\nabla L(\theta) - \nabla L(\theta')\| \leq L\|\theta - \theta'\|.$$

Assumption A.2 (Noise). There exists $\sigma^2 > 0$ such that

$$\mathbb{E}[\xi_t \mid \mathcal{F}_t] = 0, \quad \mathbb{E}[\|\xi_t\|^2 \mid \mathcal{F}_t] \leq \sigma^2.$$

Assumption A.3 (Bounded objective). $L^* := \sup_{\theta} L(\theta) < \infty$.

Assumption A.4 (Stepsize). The stepsize is constant and satisfies $\eta \leq \frac{1}{4L}$.

E.3. Alignment-Aware Convergence

Theorem E.1 (Alignment-Aware Convergence under Staleness). *Under Assumptions A.1–A.4, the iterates generated by (10)–(11) satisfy, for any $T \geq 1$,*

$$\begin{aligned} \min_{0 \leq t \leq T-1} \mathbb{E}\|\nabla L(\theta_t)\|^2 &\leq \frac{2(L^* - L(\theta_0))}{\eta T} + 2L\eta\sigma^2 + \frac{4L\eta}{T} \sum_{t=0}^{T-1} \mathbb{E}\|b_t\|^2 \\ &\quad - \frac{2}{T} \sum_{t=0}^{T-1} \mathbb{E}\langle \nabla L(\theta_t), b_t \rangle. \end{aligned} \quad (12)$$

Proof. By L -smoothness,

$$L(\theta_{t+1}) \geq L(\theta_t) + \eta \langle \nabla L(\theta_t), \hat{g}_t \rangle - \frac{L\eta^2}{2} \|\hat{g}_t\|^2.$$

Taking conditional expectation and using (11),

$$\mathbb{E}[\langle \nabla L(\theta_t), \hat{g}_t \rangle \mid \mathcal{F}_t] = \|\nabla L(\theta_t)\|^2 + \langle \nabla L(\theta_t), b_t \rangle.$$

Moreover,

$$\mathbb{E}[\|\hat{g}_t\|^2 \mid \mathcal{F}_t] \leq 2\|\nabla L(\theta_t)\|^2 + 2\|b_t\|^2 + \sigma^2.$$

Combining the above and using $\eta \leq 1/(4L)$ yields

$$\frac{\eta}{2} \mathbb{E}\|\nabla L(\theta_t)\|^2 \leq \mathbb{E}[L(\theta_{t+1}) - L(\theta_t)] - \eta \mathbb{E}\langle \nabla L(\theta_t), b_t \rangle + L\eta^2 \mathbb{E}\|b_t\|^2 + \frac{L\eta^2}{2} \sigma^2.$$

Summing over $t = 0, \dots, T-1$, telescoping, and using $L(\theta_T) \leq L^*$ gives

$$\frac{1}{T} \sum_{t=0}^{T-1} \mathbb{E}\|\nabla L(\theta_t)\|^2 \leq \frac{2(L^* - L(\theta_0))}{\eta T} + 2L\eta\sigma^2 + \frac{4L\eta}{T} \sum_{t=0}^{T-1} \mathbb{E}\|b_t\|^2 - \frac{2}{T} \sum_{t=0}^{T-1} \mathbb{E}\langle \nabla L(\theta_t), b_t \rangle.$$

The result follows by $\min_t a_t \leq \frac{1}{T} \sum_t a_t$. □

E.4. Temporal Persistence and Gradient Alignment

We now express the alignment term in (12) through temporal coupling induced by staleness.

Assumption A.5 (Bounded staleness and drift). At time t , the gradient is computed using rollouts generated at $\theta_{t-\tau_t}$ with $\tau_t \leq S$, so that

$$\theta_t - \theta_{t-\tau_t} = \sum_{k=1}^{\tau_t} \eta \hat{g}_{t-k}.$$

Assumption A.6 (Small-drift linearization). There exist matrices B_t and remainders r_t such that

$$b_t = B_t(\theta_t - \theta_{t-\tau_t}) + r_t, \quad \mathbb{E}\|r_t\| \leq \varepsilon_t.$$

Assumption A.7 (Temporal persistence). There exists $\lambda_t \geq 0$ such that

$$\mathbb{E}[\widehat{g}_{t-1}^\top B_t \widehat{g}_{t-1}] \geq \lambda_t \mathbb{E}\|\widehat{g}_{t-1}\|^2.$$

Assumption A.8 (One-step alignment stability). There exist $\rho_t \in [0, 1]$ and $\delta_t \geq 0$ such that

$$\mathbb{E}[\langle \nabla L(\theta_t), B_t \widehat{g}_{t-1} \rangle] \geq \rho_t \mathbb{E}[\widehat{g}_{t-1}^\top B_t \widehat{g}_{t-1}] - \delta_t.$$

Discussion of assumptions and empirical validation. Assumptions A.5–A.8 formalize the minimal structure needed to capture how staleness alters optimization dynamics in asynchronous GRPO. Assumption A.5 is purely structural, expressing parameter drift as the accumulation of intervening updates under bounded staleness, and holds by construction in practical asynchronous pipelines. Assumption A.6 introduces a local linearization of the staleness-induced bias, which is standard in delayed-gradient analyses and is justified as long as parameter drift remains moderate—precisely the regime prior to collapse. Assumptions A.7 and A.8 characterize temporal persistence: they require that the bias induced by stale rollouts retains nontrivial alignment with recent update directions and that this alignment does not vanish abruptly from one step to the next. Importantly, these assumptions are directional and expectation-based, rather than global or worst-case.

Our empirical results provide direct evidence supporting these assumptions. Across model scales and benchmarks, asynchronous GRPO consistently exhibits persistently elevated cosine similarity between consecutive gradients, indicating that stale gradients systematically reinforce previous update directions (supporting Assumption A.7). Moreover, the smooth evolution of alignment prior to collapse suggests that this persistence is stable across successive steps, consistent with Assumption A.8. Finally, the sharp rise in gradient alignment immediately preceding training collapse coincides with large parameter drift and breakdown of local linear behavior, aligning with the interpretation that Assumption A.6 holds in the stable regime and fails precisely when instability emerges. Together, these observations validate the assumptions as accurate descriptors of the dynamics leading to collapse, rather than as restrictive conditions imposed for analytical convenience.

Lemma E.2 (Alignment Expansion). *Under Assumptions A.5–A.6,*

$$\langle \nabla L(\theta_t), b_t \rangle = \eta \langle \nabla L(\theta_t), B_t \widehat{g}_{t-1} \rangle + \eta \sum_{k=2}^{\tau_t} \langle \nabla L(\theta_t), B_t \widehat{g}_{t-k} \rangle + \langle \nabla L(\theta_t), r_t \rangle.$$

Proof. Substitute the drift expansion into b_t and expand the inner product. □

Theorem E.3 (Convergence of Asynchronous GRPO with Alignment Persistence). *Under Assumptions A.1–A.8, the iterates satisfy*

$$\begin{aligned} \min_{0 \leq t \leq T-1} \mathbb{E}\|\nabla L(\theta_t)\|^2 &\leq \frac{2(L^* - L(\theta_0))}{\eta T} + 2L\eta\sigma^2 + \frac{4L\eta}{T} \sum_{t=0}^{T-1} \mathbb{E}\|b_t\|^2 \\ &\quad - \frac{2}{T} \sum_{t=0}^{T-1} \eta \rho_t \lambda_t \mathbb{E}\|\widehat{g}_{t-1}\|^2 + \text{Err}(T), \end{aligned} \tag{13}$$

where

$$\text{Err}(T) = \frac{2}{T} \sum_{t=0}^{T-1} \left(\eta \sum_{k=2}^{\tau_t} \mathbb{E}|\langle \nabla L(\theta_t), B_t \widehat{g}_{t-k} \rangle| + \mathbb{E}\|\nabla L(\theta_t)\| \|r_t\| + \eta \delta_t \right).$$

Proof. Apply Lemma E.2 inside Theorem E.1. The leading term is lower bounded using Assumptions A.7–A.8, while the remaining terms are controlled by absolute values and collected into $\text{Err}(T)$. □

F. Advantage of GAC: Bias Suppression via Alignment Control

The convergence bounds in Theorems E.1–E.3 show that staleness impacts optimization primarily through the bias term b_t . In particular, the penalty $\sum_t \mathbb{E} \|b_t\|^2$ is always detrimental and can dominate the bound under large staleness. Under temporal persistence (Assumptions A.5–A.8), the leading component of b_t is aligned with the previous update direction, which motivates GAC’s strategy of attenuating progress along this stale-aligned direction. We formalize this intuition by showing that projecting b_t away from $\text{span}(\hat{g}_{t-1})$ yields a strict reduction in the squared bias magnitude, up to higher-order approximation terms.

Proposition F.1 (Bias reduction via stale-direction projection). *Fix an iteration $t \geq 1$ and let \hat{g}_{t-1} be the previous stochastic gradient. Define the reference direction*

$$u_{t-1} \triangleq \begin{cases} \hat{g}_{t-1} / \|\hat{g}_{t-1}\|_2, & \hat{g}_{t-1} \neq 0, \\ 0, & \hat{g}_{t-1} = 0. \end{cases}$$

Let $P_{t-1}^\perp \triangleq I - u_{t-1} u_{t-1}^\top$ denote the orthogonal projector onto $\text{span}(u_{t-1})^\perp$.

Assume the staleness-induced bias b_t admits the one-step persistent linearization

$$b_t = \eta_{t-1} B_t \hat{g}_{t-1} + r_t, \quad (14)$$

where $B_t \in \mathbb{R}^{d \times d}$ is (possibly random) and r_t is a remainder term. Assume further the following temporal persistence condition holds:

$$\hat{g}_{t-1}^\top B_t \hat{g}_{t-1} \geq \lambda_t \|\hat{g}_{t-1}\|_2^2 \quad \text{almost surely,} \quad (15)$$

for some $\lambda_t > 0$.

Define the projected (effective) bias as

$$b_t^\perp \triangleq P_{t-1}^\perp b_t.$$

Then the following inequality holds:

$$\mathbb{E} \|b_t^\perp\|_2^2 \leq \mathbb{E} \|b_t\|_2^2 - \eta_{t-1}^2 \lambda_t^2 \mathbb{E} \|\hat{g}_{t-1}\|_2^2 + 2\eta_{t-1} \lambda_t \mathbb{E} [\|\hat{g}_{t-1}\|_2 \|r_t\|_2]. \quad (16)$$

In particular, if $\mathbb{E} \|r_t\|_2^2 \leq \epsilon_t^2$ for some $\epsilon_t \geq 0$, then

$$\mathbb{E} \|b_t^\perp\|_2^2 \leq \mathbb{E} \|b_t\|_2^2 - \eta_{t-1}^2 \lambda_t^2 \mathbb{E} \|\hat{g}_{t-1}\|_2^2 + 2\eta_{t-1} \lambda_t \epsilon_t \sqrt{\mathbb{E} \|\hat{g}_{t-1}\|_2^2}. \quad (17)$$

Proof. If $\hat{g}_{t-1} = 0$, then $u_{t-1} = 0$ and $P_{t-1}^\perp = I$, so $b_t^\perp = b_t$ and (16) holds trivially. We assume $\hat{g}_{t-1} \neq 0$ below.

Step 1: Pythagorean identity for orthogonal projection. Since P_{t-1}^\perp is an orthogonal projector, we have the decomposition

$$b_t = (u_{t-1} u_{t-1}^\top) b_t + (I - u_{t-1} u_{t-1}^\top) b_t = (u_{t-1} u_{t-1}^\top) b_t + b_t^\perp,$$

and the two components are orthogonal. Therefore,

$$\|b_t\|_2^2 = \|b_t^\perp\|_2^2 + \|(u_{t-1} u_{t-1}^\top) b_t\|_2^2. \quad (18)$$

Moreover,

$$(u_{t-1} u_{t-1}^\top) b_t = \langle b_t, u_{t-1} \rangle u_{t-1}, \quad \|(u_{t-1} u_{t-1}^\top) b_t\|_2^2 = \langle b_t, u_{t-1} \rangle^2.$$

Plugging this into (18) yields the exact identity

$$\|b_t^\perp\|_2^2 = \|b_t\|_2^2 - \langle b_t, u_{t-1} \rangle^2 = \|b_t\|_2^2 - \frac{\langle b_t, \hat{g}_{t-1} \rangle^2}{\|\hat{g}_{t-1}\|_2^2}. \quad (19)$$

Step 2: Lower bound the removed component using persistence. Using the one-step linearization (14),

$$\langle b_t, \hat{g}_{t-1} \rangle = \eta_{t-1} \hat{g}_{t-1}^\top B_t \hat{g}_{t-1} + \langle r_t, \hat{g}_{t-1} \rangle.$$

By the persistence condition (15),

$$\eta_{t-1} \hat{g}_{t-1}^\top B_t \hat{g}_{t-1} \geq \eta_{t-1} \lambda_t \|\hat{g}_{t-1}\|_2^2.$$

Also, by Cauchy–Schwarz,

$$\langle r_t, \hat{g}_{t-1} \rangle \geq -\|r_t\|_2 \|\hat{g}_{t-1}\|_2.$$

Combining the two displays gives the deterministic bound

$$\langle b_t, \hat{g}_{t-1} \rangle \geq \eta_{t-1} \lambda_t \|\hat{g}_{t-1}\|_2^2 - \|r_t\|_2 \|\hat{g}_{t-1}\|_2. \quad (20)$$

Step 3: Square and normalize. Divide (20) by $\|\hat{g}_{t-1}\|_2$ and square both sides:

$$\frac{\langle b_t, \hat{g}_{t-1} \rangle^2}{\|\hat{g}_{t-1}\|_2^2} \geq \left(\eta_{t-1} \lambda_t \|\hat{g}_{t-1}\|_2 - \|r_t\|_2 \right)^2 = \eta_{t-1}^2 \lambda_t^2 \|\hat{g}_{t-1}\|_2^2 - 2\eta_{t-1} \lambda_t \|\hat{g}_{t-1}\|_2 \|r_t\|_2 + \|r_t\|_2^2.$$

Dropping the nonnegative last term $\|r_t\|_2^2$ yields

$$\frac{\langle b_t, \hat{g}_{t-1} \rangle^2}{\|\hat{g}_{t-1}\|_2^2} \geq \eta_{t-1}^2 \lambda_t^2 \|\hat{g}_{t-1}\|_2^2 - 2\eta_{t-1} \lambda_t \|\hat{g}_{t-1}\|_2 \|r_t\|_2. \quad (21)$$

Step 4: Plug back into the projection identity and take expectation. Substitute (21) into (19):

$$\|b_t^\perp\|_2^2 \leq \|b_t\|_2^2 - \eta_{t-1}^2 \lambda_t^2 \|\hat{g}_{t-1}\|_2^2 + 2\eta_{t-1} \lambda_t \|\hat{g}_{t-1}\|_2 \|r_t\|_2.$$

Taking expectation gives (16).

Finally, if $\mathbb{E}\|r_t\|_2^2 \leq \epsilon_t^2$, then by Cauchy–Schwarz,

$$\mathbb{E}[\|\hat{g}_{t-1}\|_2 \|r_t\|_2] \leq \sqrt{\mathbb{E}\|\hat{g}_{t-1}\|_2^2} \sqrt{\mathbb{E}\|r_t\|_2^2} \leq \epsilon_t \sqrt{\mathbb{E}\|\hat{g}_{t-1}\|_2^2},$$

which yields (17). □

G. Per-Benchmark Performance Analysis

Figure 7 reports a per-benchmark breakdown of final validation accuracy for Qwen3-4B under stale-rollout training ($s=16$). Across all seven benchmarks, GAC consistently outperforms all off-policy baselines across benchmarks. Moreover, GAC achieves performance that is highly comparable to synchronized GRPO: the per-benchmark gaps remain small and do not exhibit systematic deterioration under asynchrony. Importantly, this recovery does not come from trading off learning speed for stability—GAC preserves smooth, stable convergence while maintaining a convergence rate that closely tracks the synchronized reference throughout training.

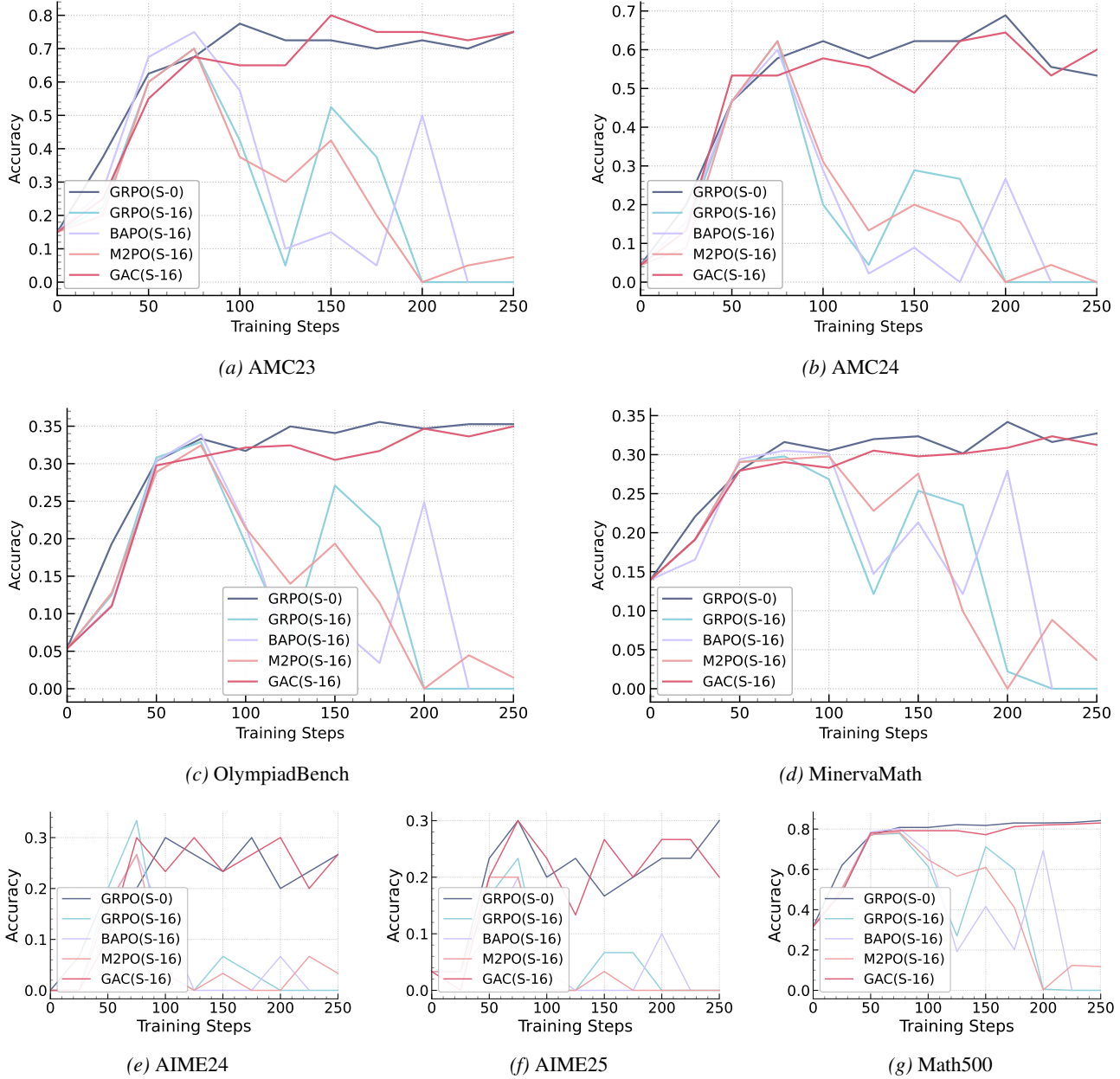


Figure 7. Per-benchmark accuracy breakdown for Qwen3-4B under staleness ($s=16$). Each panel reports final validation accuracy on one benchmark, comparing GAC against synchronized GRPO (on-policy reference) and off-policy baselines under stale rollouts.